A novel structure of silicon-on-insulator microring biosensor based on Young's two-slit interference and its simulation*

Su Baoqing(苏保青), Wang Chunxia(王春霞)†, Kan Qiang(阚强), Li Junhua(李俊华), Xie Yiyang(解意洋), Wang Zhenzhen(王真真), and Chen Hongda(陈弘达)

State Key Laboratory Integrated Optoelectronics, Institute of Semiconductors, Chinese Academy of Sciences, Beijing 100083, China

Abstract: A novel silicon-on-insulator microring biosensor based on Young's twoslit interference has been demonstrated. The transducer signal from electric field intensity distribution on the interference screen is given by using the transfer matrix method (TMM) and two-slit interference principle. The result shows that the structure we propose is advantageous for sensing as the interference pattern is very sensitive to the ambient refractive index around the microring. A small perturbation in refractive index around the microring Δn_c will result in a notable shift of destructive interference points (DIPs) on the interference screen. By detecting the shift of the DIPs, the ambient refractive index change can be obtained.

Key words: silicon-on-insulator; microring; Young's two-slit interference; biosensor
DOI: 10.1088/1674-4926/32/7/074010 **EEACC:** 4140; 4145

1. Introduction

The optical biosensor is an important detection and analysis tool that has been widely used in many applications, such as biomedical research, healthcare, pharmaceuticals, and environmental monitoring[1−4]. Compared with electrical sensors, optical sensors have unique merits, e.g., immune to electro–magnetic interference, capable of remote sensing and multiple-matter detection within a single device. Typically, there are two detection methods that can be implemented in optical biosensing: fluorescence-based detection and label-free detection[5]. Fluorescence-based detection is extremely sensitive down to single molecule detection[6]. However, it suffers from the labeling process, which is laborious and expensive. In contrast, label-free detection is relatively easy and cheap, and can perform quantitative measurements. So quantitative and label-free monitoring of the molecule is advantageous in many applications.

Integrated ring resonators were first proposed by Marcatili in 1969 at Bell Labs[7]. The layout he proposed can be regarded as the standard configuration for an integrated resonator channel dropping filter. However, research on optical microring resonators has been improving slowly for a long time because of the limitation of surface microfabrication technology. In recent years, with the rapid improvement of materials science and surface microfabrication technology, microring resonators with various materials and structures have been proposed. Barrios has proposed a silicon nitride slot-waveguide microring resonator[8], in which high optical intensity is obtained in the slot region, making the slot-waveguide very attractive for RI sensing due to its capability of enhancing sample-probe interaction. Several new structures of microring resonator based on SOI have been proposed that are optimized for sensing: increasing the Q factor by enlarging sensing cavity length[9] or enhancing the notch depths by concentric microring resonators[10]. Compared with other optical sensors[11], microring resonator sensors can provide ultracompact size and easy realization of a sensor array, especially for waveguides based on silicon-on-insulator (SOI) materials due to the high index contrast, which is suitable for the fabrication of a nanophotonic waveguide including a submicron sized optical cavity with high quality[12−16]. In this paper, a sensor structure based on a microring is proposed. The structure incorporates a Y-shape splitter with one branch side-coupled by a microring, and the other serves as a reference arm. Output light from two branches interfere with each other in the free space, and the interference pattern is captured by a CCD detector. Compared with typical microring biosensors, the structure we propose has unique advantages. First, it combines the mode resonance and waveguide interference, which makes the spectrum analysis unnecessary, and reduces the volume of the device. Second, a CCD detector is used in the sensor configuration, which realizes real-time monitoring. The analytical description of electric field intensity distribution on the interference screen is derived. Our investigation shows that the interference pattern is very sensitive to the ambient refractive index n_c. And the refractive index change can be valued quantitatively by detecting the DIPs shift.

2. Structure and mechanism

A schematic of the sensor is shown in Fig. 1. The sensor we propose contains a plane waveguide chip with one microring-coupled Y splitter and a CCD detector serving as an interfer-

* Project supported by the National Natural Science Foundation of China (Nos. 60736037, 60978067, 60807010, 61036009), the National Basic Research of China (Nos. 2009CB320300, 2010CB934104), and the National High Technology Research and Development Program of China (No. 2009AA03Z412).

† Corresponding author. Email: cxwang@semi.ac.cn

Received 24 December 2010, revised manuscript received 28 March 2011

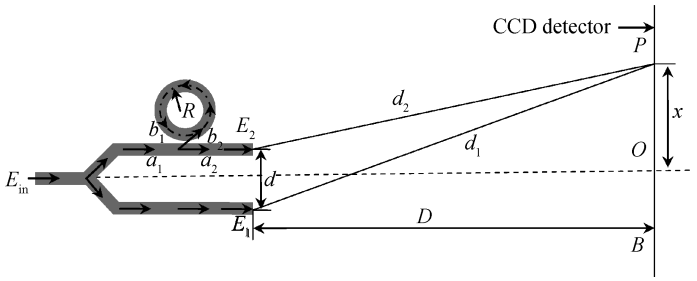

Fig. 1. Schematic of microring resonator sensor based on Young's two-slit interference.

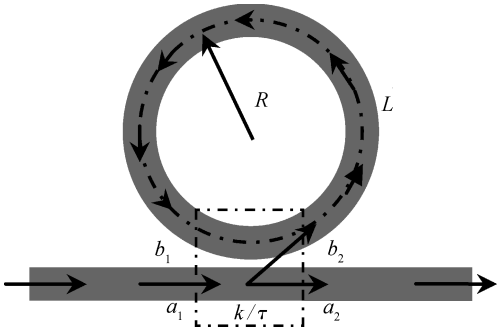

Fig. 2. Schematic of a typical all-pass ring resonator.

ence screen. Input light is split into two beams equally. Light transmitting in branch 2 is coupled into the microring when the microring resonance condition is satisfied. Then the resonated light is coupled out of the microring and the microring resonance causes a phase delay. The light from branch 2 of Y splitter interferes with reference branch 1 in the free space, and the interference pattern is collected by a CCD detector.

The structure in Fig. 2 is a typical all-pass ring resonator. Light satisfying the resonance condition will be coupled into the microring. The resonance condition can be expressed as

$$m\lambda = N_{\text{eff}}L, \tag{1}$$

where λ is the resonance wavelength, m is the cavity resonance order (= 1, 2, 3, ...), N_{eff} is the effective index of the ring waveguide, and L is the length of the microring. The basic relations amongst the incident a_1, transmitted a_2, and circulating b_1, b_2 fields within the microring resonator are derived using the transfer matrix method (TMM).

$$\begin{aligned} &\begin{pmatrix} a_2 \\ b_2 \end{pmatrix} = \begin{pmatrix} \tau & ik \\ ik & \tau \end{pmatrix} \begin{pmatrix} a_1 \\ b_1 \end{pmatrix}, \\ &b_1 = \exp(-\alpha L + i\omega T) b_2, \end{aligned} \tag{2}$$

where τ and k are coupling coefficient and transmitting coefficient, respectively. α is the loss coefficient of the ring cavity waveguide (i.e. no loss corresponds to $\alpha = 1$), ω is the optical frequency and T is the transit time of one round trip for the microring, which can be obtained by $T = N_{\text{eff}}L/c$. We can get the normalized transmission equation, which is

$$\frac{a_2}{a_1} = \frac{\tau - A\exp(i\phi)}{1 - \tau A\exp(i\phi)}, \tag{3}$$

where A is the field attenuation of the microring for one round trip, and one has $A = \exp(-\alpha L)$, ϕ represents the phase delay for one round trip, and one has $\phi = \omega T$. The effective phase delay Φ caused by the microring resonator is defined as the phase argument of the field transmission factor, which is

$$\Phi = \pi + \phi + \arctan\frac{\tau\sin\phi}{A - \tau\cos\phi} + \arctan\frac{A\tau\sin\phi}{1 - A\tau\cos\phi}. \tag{4}$$

At the resonance wavelengths of the microring, we have $\phi = \omega T = (2\pi c/\lambda) \times (N_{\text{eff}}L/c) = 2m\pi$, so $\Phi = (2\,m + 1)\pi$.

In Fig. 1, we suppose that the two branches have the same length, so the phase delay caused by the two branches of the Y splitter is defined as θ. At the output ports, the phase from two branches can be written as

$$\begin{cases} \Phi_1 = \theta, \\ \Phi_2 = \pi + \phi + \theta \\ \qquad + \arctan\dfrac{\tau\sin\phi}{A - \tau\cos\phi} + \arctan\dfrac{A\tau\sin\phi}{1 - A\tau\cos\phi}. \end{cases} \tag{5}$$

So the phase difference between the two output ports is

$$\begin{aligned} \delta_1 = \Phi_2 - \Phi_1 = \pi + \phi + \arctan\frac{\tau\sin\phi}{A - \tau\cos\phi} \\ + \arctan\frac{A\tau\sin\phi}{1 - A\tau\cos\phi}. \end{aligned} \tag{6}$$

Light from two branches interfere with each other in the free space, and the interference pattern is detected by a CCD detector. The phase difference from two output ports of the waveguides to the interference screen is

$$\delta_2 = \frac{2\pi}{\lambda}(d_1 - d_2) = \frac{2\pi}{\lambda}\Delta, \tag{7}$$

where d_1 and d_2 are

$$d_1 = \sqrt{\left(x + \frac{d}{2}\right)^2 + D^2}$$

and

$$d_2 = \sqrt{\left(x - \frac{d}{2}\right)^2 + D^2}.$$

So

$$\Delta = d_1 - d_2 = \frac{d_1^2 - d_2^2}{d_1 + d_2} = \frac{2xd}{d_1 + d_2},$$

where d_1 and d_2 are the distances from the two output ports of the waveguides to the detection point (P), respectively. Parameter d is distance Y splitter, and D is the distance from output port of waveguide to the interference screen. If $D \gg d$, then $\Delta = xd/D$, and the phase difference from two output ports of the waveguides to the interference screen will be

$$\delta_2 = \frac{2\pi}{\lambda}(d_1 - d_2) = \frac{2\pi d}{\lambda D}x. \tag{8}$$

The overall phase difference can be written as

$$\delta = \delta_1 + \delta_2 = \pi + \phi + \arctan\frac{\tau\sin\phi}{A - \tau\cos\phi} + \arctan\frac{A\tau\sin\phi}{1 - A\tau\cos\phi} + \frac{2\pi d}{\lambda D}x. \tag{9}$$

We consider the situation where the microring waveguide is lossless, that is $A = 1$, then from Eq. (3) we have $a_1 = -a_2$. So the energy from the two branches is the same $I_1 = I_2 = I/2$, where I_1 and I_2 are electric intensity from two output ports, respectively, and I is input intensity. Suppose $I = 1$, then the intensity distribution on the interference screen can be obtained by

$$I = I_1 + I_2 + 2\sqrt{I_1 I_2}\cos\delta = I(1 + \cos\delta) = 1 + \cos\delta. \tag{10}$$

From Eqs. (9) and (10), we can see that, when the ambient refractive index around the microring n_c varies, the effective refractive index N_{eff} will be changed. From Eq. (1), for a fixed operating wavelength, the resonance condition will be dissatisfied, and the overall phase difference δ will be changed, which will result in a shift in intensity distribution on the interference screen.

3. Results and discussion

In this part, we study the relationship between the shift of DIPs on the CCD screen and the ambient refractive index change Δn_c around the microring resonator. We take the rib waveguide, for example, to study the influence of microring parameters on the sensing performance of the microring-based sensor.

Suppose the microring waveguide is fabricated on an SOI substrate, with 340 nm top Si ($n_{\text{Si}} = 3.445$) layer and 1 μm SiO_2 ($n_{SiO_2} = 1.445$) layer, and a rib waveguide with rib height of 230 nm and rib width of 500 nm. TM polarization is considered, which is more sensitive to the changes of ambient refractive index than TE polarization[16].

First, we calculate the electric field intensity distribution on the interference screen. Suppose the refractive index of the microring superstrate is n_1, the resonance wavelength is λ, and the cavity resonance order is m. From Eq. (9), we can see that, at the resonance wavelength λ, the phase difference δ is

$$\delta = (2m + 1)\pi + \frac{2\pi d}{\lambda D}x, \tag{11}$$

and the intensity distribution on the interference screen is

$$I = 1 - \cos\left(2m\pi + \frac{2\pi d}{\lambda D}x\right), \tag{12}$$

we can see that the energy on interference screen is distributed in cosine function of x. At the position of $x = 0$, the electric intensity is zero, which corresponds to a DIP on the interference screen. This is opposite to the Young's two-slit interferometer, in which the point of $x = 0$ is always a constructive interference point (CIP).

If $I(P) = 0$, we can get the DIPs at

$$x = \frac{\lambda D}{\pi d}(n\pi - m\pi), \tag{13}$$

where n is the extinction order of the interference pattern.

Then, if the index of the microring superstrate changes to n_2, then $\Delta n_c = n_2 - n_1$. The resonance wavelength will shift to λ', and the effective index of the microring waveguide will change by ΔN_{eff}. The DIP will shift from x to x' for the extinction order of n. Within a small wavelength range, the effective index change ΔN_{eff} is almost proportional to the ambient index change Δn_c[18], so $\Delta N_{\text{eff}} = K\Delta n_c$, where the parameter K is constant and depends on the material and waveguide cross-section, then

$$\phi' = \omega T = \frac{2\pi c}{\lambda}\frac{(N_{\text{eff}} + \Delta N_{\text{eff}})L}{c} = 2m\pi\left(1 + \frac{K\Delta n_c}{N_{\text{eff}}}\right), \tag{14}$$

and

$$\delta' = \pi + \phi' + 2\arctan\frac{\tau\sin\phi'}{1 - \tau\cos\phi'} + \frac{2\pi d}{\lambda D}x. \tag{15}$$

So the energy distribution on the interference screen is

$$I(P) = 1 + \cos\delta' = 1 - \cos\left(\phi' + 2\arctan\frac{\tau\sin\phi'}{1 - \tau\cos\phi'} + \frac{2\pi d}{\lambda D}x\right). \tag{16}$$

From Eqs. (14) –(16), we can see that the $I(P)$ is a function of Δn_c and x. We suppose the radius of microring (R) is 5 μm. The distance between the two waveguide branches (d) is 20 μm, and the distance from the output waveguide to the interference screen (D) is 5 cm. When n_c changes from 1.33 to 1.34, the effective index of the microring waveguide (N_{eff}) will change from 2.5273 to 2.5287 at the resonance wavelength of 1.58795 μm. Based on the mode effective index calculation of the rib waveguides, we obtain the parameter $K = \Delta N_{\text{eff}}/\Delta n_c = 0.14$. Figure 3 shows the electric field intensity distribution on the interference screen as a function of x with $n_c = 1.33$ (the solid line) and 1.34 (the symbol line), respectively. We can see that the DIP at $x = 0$ cm is shifted to -0.06 cm when the ambient refractive index changed to 1.34, which can be easily detected by a CCD detector.

If we suppose $I(P) = 0$, we can get the relationship between DIPs position x' and Δn_c, which is

$$x' = \frac{\lambda D}{2\pi d}\left(2n\pi - \phi' - 2\arctan\frac{\tau\sin\phi'}{1 - \tau\cos\phi'}\right), \tag{17}$$

where n is the extinction order of the interference pattern. From Eqs. (13), (14) and (17), we can get the shift of DIPs of the same extinction order Δx.

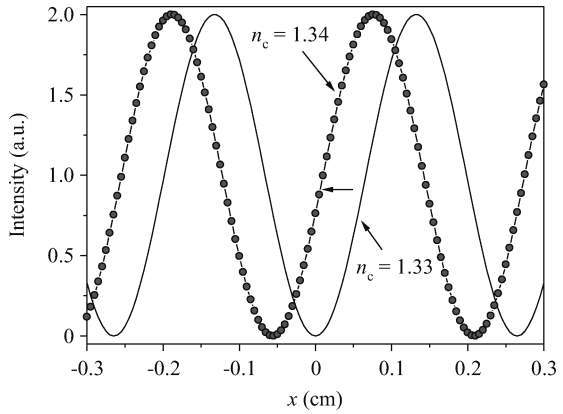

Fig. 3. Electric field intensity distribution on the interference screen as a function of x with $n_c = 1.33$ (the solid line) and 1.34 (the symbol line), respectively.

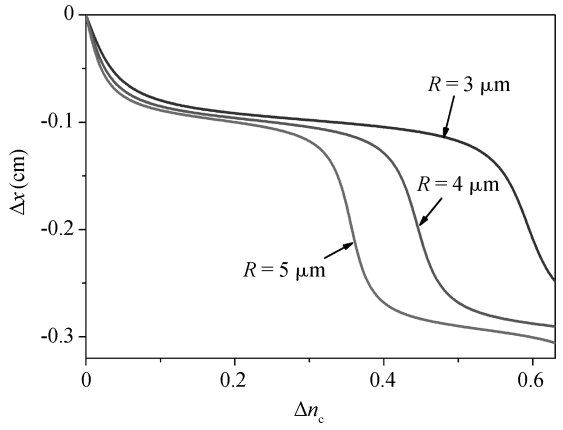

Fig. 4. Extinction point shift Δx as a function of Δn_c with a microring radius of 3 μm, 4 μm, 5 μm, respectively.

$$\Delta x = x' - x = -\frac{\lambda D}{\pi d}\left[m\pi K\Delta n_c/N_{\text{eff}} + \arctan\frac{\tau\sin(2m\pi K\Delta n_c/N_{\text{eff}})}{1-\tau\cos(2m\pi K\Delta n_c/N_{\text{eff}})}\right]. \quad (18)$$

From Eq. (18), we can see that the cavity resonance order m and transmitting coefficient τ are two important parameters, where parameter m will restrict the measurement range of refractive index, and τ will influence the sensitivity of the sensor. The cavity resonance order m is associated with the microring radius R by $m\lambda = N_{\text{eff}}L$. Figure 4 shows the DIPs shift Δx as a function of Δn_c with a microring radius of 3 μm, 4 μm, 5 μm, respectively. We can see that as the radius increases, the measurement range of the effective index is getting small. So a small radius microring is needed for a large dynamic measurement range.

The transmitting coefficient τ is related to the coupling coefficient k by $k^2 + \tau^2 = 1$. The coupling coefficient k determines the fraction of light coupling into the microring. The DIPs shift Δx as a function of Δn_c is shown in Fig. 5 for transmitting coefficients $\tau = 0.3$, 0.5, 0.7, and 0.9. We can see that

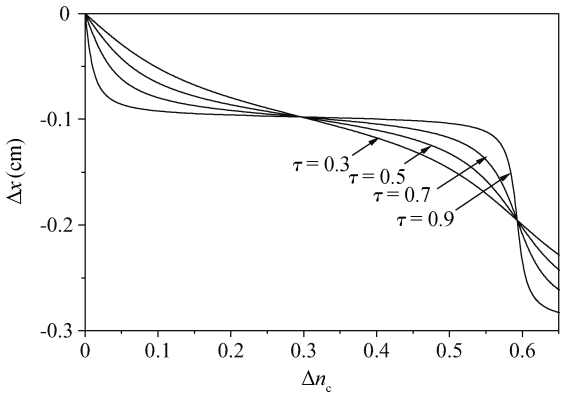

Fig. 5. DIPs shift Δx as a function of Δn_c for transmitting coefficients $\tau = 0.3$, 0.5, 0.7, and 0.9, respectively.

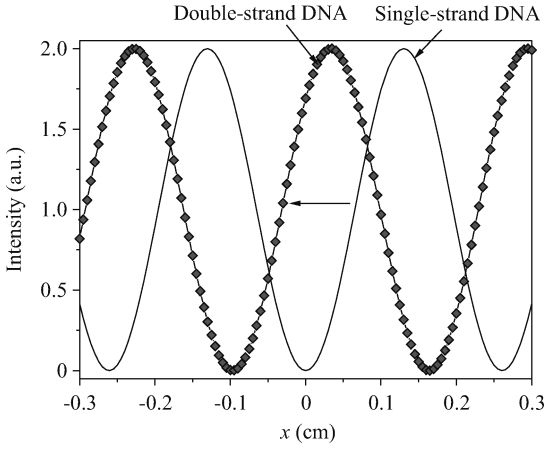

Fig. 6. Electric field intensity distribution on the interference screen as function of x with single-strand DNA (the solid line) and double-strand DNA (the symbol line).

as the transmitting coefficient increases, the curves' slope at $\Delta n_c = 0$ and 0.6 becomes large, and between the two positions, the curve is getting flat, which is not suitable for sensing. Therefore, a small transmitting coefficient is needed.

From the results above, we can see that, the sensor structure we proposed can be optimized for sensing application by reducing the radius of microring or choosing a large coupling coefficient.

4. Biosensing application with the proposed device

Biomolecular detection is an important process in bioanalysis and biomonitoring. In this part, a DNA hybridization process will be simulated using the proposed sensor configuration. We study the DIPs shift when the single-strand DNA is hybridized into double-strand DNA. We assume that the single-strand DNA (50 nm thickness) is initially immobilized on the silicon layer around the microring resonator as the probe. The interference pattern is detected by a CCD detector at the interference screen. Then we will study the interference pattern shift as the hybridization proceeds. The refractive indices of single-strand DNA and double-strand DNA layers are around 1.456 and 1.53, respectively, with a binding density of 1.49

pmol/cm^2[19, 20]. The effective refractive index of the waveguide changes from 2.540161 (before DNA hybridization) to 2.544190 (after DNA hybridization). Figure 6 shows the electric field intensity distribution on the interference screen as a function of x with single-strand DNA (solid line) and double-strand DNA (symbol line). We can see that the interference pattern exhibits a notable shift after DNA hybridization. For example, the DIP at $x = 0$ (before DNA hybridization) shifts about 0.1 cm after DNA hybridization, which can be easily detected by CCD detector.

5. Conclusion

In conclusion, we have presented our work in developing a SOI microring resonator for sensing applications, in which the sensor is based on Young's two-slit interference configuration. Through TMM (transfer matrix method) calculations and the two-slit interference principle, we have given a detailed analysis of the intensity distribution on the interference screen. The destructive interference point (DIP) on the interference screen will shift as the refractive index around microring n_c changes. Our study reveals that the interference pattern is very sensitive to refractive index change. A small perturbation in n_c will result in a notable shift in DIPs on the interference screen. By detecting the shift in DIPs, the ambient refractive index change can be obtained. Our study shows that the sensor structure can be optimized by reducing the radius of the microring or choosing a large coupling coefficient of the microring. The sensor structure we proposed can be fabricated by cheap semiconductor technology and has potential application by integrating a signal process system and is suited for mass-scale production.

References

[1] Narayanaswamy R, Wolfbeis O S. Optical sensors. New York: Springer, 2004
[2] Vahala K J. Optical microcavities. Nature, 2003, 424: 839
[3] Vollmer F, Arnold S. Whispering-gallery-mode biosensing: label-free detection down to single molecules. Nat Methods, 2008, 5(7): 591
[4] Armani M, Kulkarni R K, Fraser S E, et al. Label-free, single-molecule detection with optical microcavities. Science, 2007, 317(5839): 783
[5] Fan X, White I M, Shopova S I, et al. Sensitive optical biosensors for unlabeled targets: a review. Anal Chim Acta, 2008, 620: 8
[6] Moerner W E. Principal-components analysis of shape fluctuations of single DNA molecules. Proc Natl Acad Sci, 2007, 104: 12596
[7] Marcatili E A J. Bends in optical dielectric guides. The Bell System Technical Journal, 1969, 48: 2103
[8] Barrios C A. Analysis and modeling of a silicon nitride slot-waveguide microring resonator biochemical sensor. Opt Sensors. 2009, 7356(1):735605
[9] Xu D X, Densmore A, Delâge A, et al. Folded cavity SOI microring sensors for high sensitivity and real time measurement of biomolecular binding. Opt Express, 2008, 16(19): 15137
[10] Li X H, Zhang Z Y, Qin S Y, et al. Sensitive label-free and compact biosensor based on concentric silicon-on-insulator microring resonators. Appl Opt, 2009, 48(25): F90
[11] Anderson G P, Golden J P, Ligler F S. A fiber optic biosensor: combination tapered fibers designed for improved signal acquisition. Biosens Bioelectron, 1993, 8: 249
[12] Densmore A, Xu D X, Waldron P, et al. A silicon-on-insulator photonic wire based evanescent field sensor. IEEE Photonics Technol Lett, 2006, 18: 2520
[13] Tiefenthaler K, Lukosz W. Sensitivity of grating couplers as integrated-optical chemical sensors. J Opt Soc Am B, 1989, l6(2): 209
[14] Veldhuis G J, Parriaux O, Hoekstra H J W, et al. Sensitivity enhancement in evanescent optical waveguide sensors. J Lightwave Technol, 2000, 18(5): 677
[15] Parriaux O, Veldhuis G J. Normalized analysis for the sensitivity optimization of integrated optical evanescent-wave sensors. J Lightwave Technol, 1998, 16(4): 573
[16] Chao Y, Guo L J. Polymer microring resonators for biochemical sensing applications. IEEE J Sel Topics Quantum Electron, 2006, 12(1): 134
[17] Xu D X, Densmore A, Delâge A, et al. Folded cavity SOI microring sensors for high sensitivity and real time measurement of biomolecular binding. Opt Express, 2008, 16(19): 15137
[18] Dai D, He S. Highly sensitive sensor with large measurement range realized with two cascaded microring resonators. Opt Commun, 2007, 279: 89
[19] Elhadj S, Singh G, Saraf R F. Optical properties of an immobilized DNA monolayer from 255 to 700 nm. Langmuir, 2004, 20: 5539
[20] Mandal S, Erickson D. Nanoscale optofluidic sensor arrays. Opt Express, 2008, 16: 1623